EcoMat

WILEY

EcoMat
FUNCTIONAL MATERIALS FOR GREEN ENERGY AND ENVIRONMENT

RESEARCH ARTICLE OPEN ACCESS

A LiFSI-Based Ultralight Electrolyte for Long-Cycle-Life and High-Energy-Density Lithium-Sulfur Batteries

Junhua Zhou[1,2] | Yufeng Luo[1,2] | Chao Wang[1,2] | Chuan Xie[1,2] | Huimin Wang[1,2] | Yanpeng Guo[1,2] | Yongqiang Yang[1,2] | Zhibo Li[1,2] | Shujing Wen[1,2] | Jiehua Cai[3] | Qiyao Huang[3,4] | Zijian Zheng[1,3,4,5,6]

[1]Department of Applied Biology and Chemical Technology, The Hong Kong Polytechnic University, Hong Kong SAR, China | [2]School of Fashion and Textiles, The Hong Kong Polytechnic University, Hong Kong SAR, China | [3]Research Institute for Intelligent Wearable Systems, The Hong Kong Polytechnic University, Hong Kong SAR, China | [4]Research Institute for Smart Energy, The Hong Kong Polytechnic University, Hong Kong SAR, China | [5]PolyU-Daya Bay Technology and Innovation Research Institute, Huizhou, China | [6]PolyU-Wenzhou Technology and Innovation Research Institute, Wenzhou, China

Correspondence: Zijian Zheng (tczzheng@polyu.edu.hk)

Received: 30 November 2025 | **Revised:** 8 January 2026 | **Accepted:** 19 January 2026

Keywords: high energy density | LiFSI | lithium-sulfur batteries | long cycle life | ultralight electrolytes

ABSTRACT

Lithium-sulfur (Li-S) batteries are promising candidates for high-energy storage; however, the high electrolyte uptake of porous S cathodes significantly limits their practical energy density. Although ultralight electrolytes (ULEs) can address this issue, they often suffer from low ionic conductivity, unstable interphases, and sluggish kinetics. This study presents a ULE design based on lithium bis(fluorosulfonyl)imide (LiFSI) salt, which simultaneously achieves a low density (0.89 g cm^{-3}) and high Li^+ conductivity (7.05 mS cm^{-1}). The LiFSI salt facilitates the formation of a LiF-rich solid electrolyte interphase on the Li metal anode, effectively suppressing polysulfide corrosion and enhancing cycle life. Furthermore, its high donor number improves polysulfide solubility, accelerating conversion kinetics and increasing capacity utilization. As a result, high-loading S cathodes (5 mg cm^{-2}) deliver an initial capacity of 1180 mAh g^{-1} and retain 70.63% of this capacity after 200 cycles. Pouch cells with the LiFSI-ULE exhibit a 34.5% higher energy density and a 133% longer cycle life compared to those with conventional electrolytes. This study successfully extends the application of LiFSI to Li-S batteries, offering a viable pathway toward long-cycling, high-energy-density energy storage.

1 | Introduction

Lithium-sulfur (Li-S) batteries are among the most promising next-generation energy storage technologies, primarily due to their exceptionally high theoretical energy density (2600 Wh kg^{-1}) and the natural abundance and low cost of S [1–4]. However, the intrinsic insulating nature of S (~1×10^{-15} S/m) necessitates the fabrication of highly porous carbon/sulfur composite cathodes to ensure adequate electrical conductivity [5–8]. This high porosity, in turn, requires a large amount of electrolyte for effective wetting. Even under lean electrolyte conditions—for example, with an electrolyte-to-sulfur (E/S) ratio as low as 4 μL mg^{-1}—the electrolyte can constitute up to 68.5 wt.% of the total cell weight, a figure substantially higher than that in commercial lithium-ion batteries (< 25 wt.%) [9–13]. Consequently, this excessive electrolyte weight severely compromises the practical energy density of Li-S batteries, posing a major challenge to their commercialization.

The application of ultralight electrolytes (ULEs) offers a promising strategy to enhance the practical energy density of Li-S batteries. For example, reducing the electrolyte density from the commercial standard of 1.2 g mL^{-1} to 0.8 g mL^{-1} could significantly increase the estimated energy density from 392 to 531 Wh kg^{-1}, as shown in Figure 1a. To achieve this, several studies have attempted to design ULEs by either lowering the

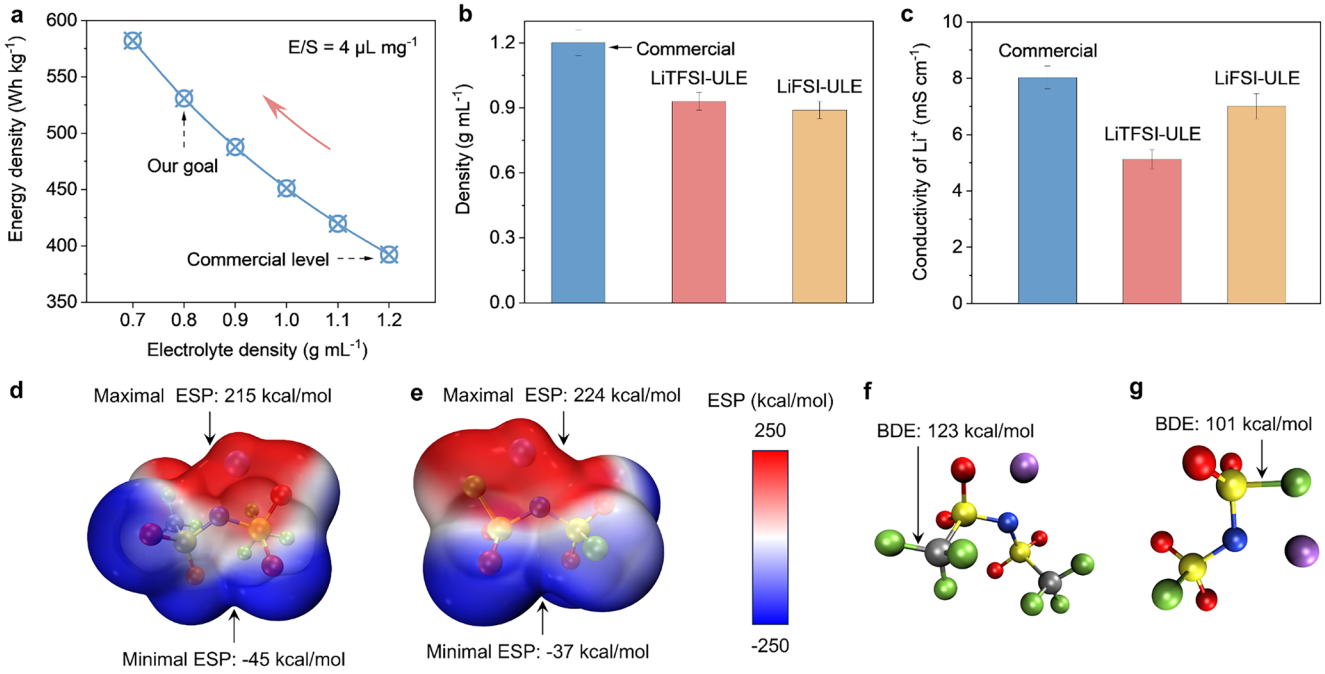

FIGURE 1 | Design strategy and physicochemical properties of ultralight electrolytes (ULEs). (a) The critical relationship between electrolyte density and achievable battery energy density, establishing the target for ULE design at E/S = 4 mL g^{-1}. (b, c) The formulated LiTFSI-ULE and LiFSI-ULE electrolytes exhibit favorable physical properties compared to the commercial benchmark, including (b) density and (c) conductivity. (d, e) Molecular-level analysis via electrostatic potential (ESP) mapping reveals distinct charge distributions in (d) LiTFSI and (e) LiFSI, while (f, g) the lower bond dissociation energy (BDE) of the S-F bond in (g) LiFSI suggests a different degradation pathway compared to the C-F bond in (f) LiTFSI.

concentration of the conventional lithium bis(trifluoromethanesulfonyl)imide (LiTFSI) salt or developing low-density solvents [10, 14, 15]. However, the performance of these reported ULEs remains unsatisfactory, particularly when paired with high-sulfur-loading cathodes (≥4 mg cm^{-2}). This underperformance arises from three primary challenges. First, low-concentration (<1 M) LiTFSI results in insufficient Li^+ ion conductivity, leading to poor capacity utilization, especially in practical, thick S cathodes [16, 17]. Second, the reduced amount of LiTFSI salt causes the formation of a fragile solid electrolyte interphase (SEI) on the Li metal anode, which exacerbates corrosion by polysulfides and consequently shortens the battery's cycle life [15, 18]. Third, the currently reported low-density solvents are predominantly single-oxygen ethers, which exhibit poor polysulfide solubility, resulting in sluggish conversion kinetics and low S utilization [19, 20]. Therefore, it is essential to develop new Li salts or solvents that can produce ULEs with high Li^+ conductivity, effective interphase-forming capability, and moderate polysulfide dissolution ability.

In comparison, lithium bis(fluorosulfonyl)imide (LiFSI) emerges as a more promising Li salt for developing high-performance ULEs. LiFSI offers several intrinsic advantages over LiTFSI. Primarily, its lower molecular weight (187 g mol^{-1} versus 287 g mol^{-1} for LiTFSI) directly contributes to a reduction in electrolyte density at equivalent concentrations. Furthermore, LiFSI-based electrolytes exhibit higher Li^+ ion conductivity, a critical attribute for low-concentration ULEs where ionic transport often limits performance [21, 22]. Additionally, LiFSI facilitates the formation of a stable, LiF-rich SEI on the Li metal anode, which is pivotal for achieving higher Coulombic efficiency (CE) and mitigating dendrite growth [23, 24]. Despite these compelling benefits, the application of LiFSI in Li-S batteries has been scarcely reported. This notable gap arises from a fundamental incompatibility: LiFSI is known to initiate the polymerization of 1,3-dioxolane (DOL), a common cosolvent in Li-S electrolytes, leading to the formation of poly(DOL) [25]. This polymer can impede Li^+ diffusion, resulting in poor rate capability and diminished fast-charging performance. Consequently, the considerable potential of LiFSI to address key challenges in Li-S batteries remains largely unexplored.

Herein, we report the rational design of a LiFSI-based ultralight electrolyte (LiFSI-ULE) that effectively overcomes the aforementioned limitations of conventional ULEs in Li-S batteries. This novel electrolyte formulation simultaneously achieves an ultralow density of 0.89 g mL^{-1} and a high Li^+ conductivity of 7.05 mS cm^{-1}. The strategic use of LiFSI confers dual synergistic benefits. On the Li metal anode side, the derived LiF-rich SEI effectively suppresses polysulfide corrosion, thereby enhancing CE and extending cycle life. On the S cathode side, the high donor number of the FSI^- anion improves polysulfide solubility, which accelerates the conversion kinetics and boosts S utilization. As a result, under practical conditions with a high S loading (5 mg cm^{-2}) and a low E/S ratio (5 mL g^{-1}), the LiFSI-ULE enables a high initial capacity of 1180 mAh g^{-1} and capacity retention of 70.63% after 200 cycles at 0.5 C (1 C = 1000 mA g^{-1}). This performance is superior to all previously reported results employing electrolyte modification strategies under analogous practical test conditions. Furthermore, pouch cells configured with an ultrahigh S loading (8 mg cm^{-2}) and a lean E/S ratio of 4 μL mg^{-1} demonstrate a 34.5% higher energy density and a 133% longer cycle

life compared to those using commercial electrolytes. This study not only successfully extends the application of LiFSI to the Li-S battery system but also provides a viable and promising path toward achieving long-cycling, high-energy-density storage.

2 | Results and Discussion

2.1 | Electrolyte Formulation and Physicochemical Properties

The density of an electrolyte is determined by three primary factors: the density of the solvents, the concentration, and the molecular weight of the Li salt. To engineer an ultralight electrolyte, we systematically modified a conventional commercial electrolyte (1 M LiTFSI and 0.1 M $LiNO_3$ in a 1:1 v/v mixture of 1,2-dimethoxyethane (DME) and DOL). The LiFSI-ULE (0.4 M LiFSI and 0.1 M $LiNO_3$ in DME) was formulated by strategically (1) eliminating the relatively dense DOL solvent (1.06 g mL^{-1}), (2) replacing the high-molecular-weight LiTFSI salt (287 g mol^{-1}) with the lighter LiFSI alternative (187 g mol^{-1}), and (3) reducing the total salt concentration. This rational design resulted in a significant reduction in density, from 1.2 g mL^{-1} for the commercial electrolyte to just 0.89 g mL^{-1} for the LiFSI-ULE, as quantitatively shown in Figure 1b. For a controlled comparison to elucidate the specific role of the LiFSI salt, a LiTFSI-based ultralight electrolyte (LiTFSI-ULE) with the same salt concentration (0.4 M LiTFSI and 0.1 M $LiNO_3$ in DME) was also prepared, exhibiting a density of 0.92 g mL^{-1}. The rationale for selecting the 0.4 M concentration is based on the comprehensive electrochemical data (Figures S1 and S2).

As expected, reducing the salt concentration led to a sharp decrease in conductivity, which dropped from 8.02 mS cm^{-1} in the commercial electrolyte to 5.13 mS cm^{-1} in the LiTFSI-ULE (Figure 1c). Impressively, the LiFSI-ULE exhibited a significantly enhanced conductivity of 7.05 mS cm^{-1}, a value close to that of the commercial electrolyte. This superior transport property was further supported by a higher Li^+ transference number (0.45 vs. 0.43) and a larger exchange current density (150 μA cm^{-2} vs. 110 μA cm^{-2}) compared to the LiTFSI-ULE (Figures S3 and S4), collectively indicating accelerated electrode kinetics.

To elucidate the origin of this high conductivity, we analyzed the electrostatic potential (ESP) of the anions. The ESP maps reveal a more localized charge distribution in LiFSI, indicating that it is a more polar molecule than LiTFSI (Figure 1d,e). This increased polarity suggests a weaker Coulombic interaction between the Li^+ cation and the FSI^- anion, thereby facilitating easier dissociation and contributing to higher ionic conductivity. Conversely, the more negative minimum ESP of LiTFSI (−45 kcal mol^{-1} vs. −37 kcal mol^{-1} for LiFSI) implies a stronger electron density on its oxygen atoms, which likely enhances coordination with Li^+ ions, resulting in a lower degree of dissociation and reduced conductivity. Furthermore, the maximum ESP of LiFSI is approximately 9 kcal mol^{-1} higher, indicating greater susceptibility to reductive decomposition on the Li metal anode. This observation aligns with bond dissociation energy (BDE) data showing that the S-F bond in LiFSI is significantly weaker (~22 kcal mol^{-1}) than the C-F bond in LiTFSI (Figure 1f,g), a characteristic that promotes the formation of a robust, LiF-rich SEI.

2.2 | Corrosion Behavior of Lithium Metal Anodes in Li-S Batteries

The electrochemical performance of the designed electrolytes was initially evaluated in Li-S coin cells configured with low-sulfur-loading cathodes (~1 mg cm^{-2}, Figure S5) to elucidate their fundamental behavior. After two formation cycles at 0.1 C, the cells were cycled at 1 C. While the S cathode in the LiTFSI-ULE exhibited higher capacity retention (79.87%) than the commercial electrolyte (68.64%) despite a similar initial capacity of approximately 915 mAh g^{-1} (Figures 2a and S6), its CE was consistently less than 100% throughout cycling, decreasing from 99.36% in the first cycle to 97.59% by the 100th cycle (Figure 2b). This steadily decreasing CE clearly indicates continuously deteriorating polysulfide shuttle effects especially at high loading of S (Figure S7). In stark contrast, the LiFSI-ULE enabled both the highest initial capacity utilization (1084 mAh g^{-1}) and the best capacity retention (91.16%). Crucially, it also maintained a near-ideal average CE of 99.97%, which was superior even to the commercial electrolyte (99.91%). These CE trends were directly corroborated by chronopotentiometry measurements, which revealed corresponding shuttle currents of 36 μA, 55 μA, and 29 μA at 2.3 V for the commercial, LiTFSI-ULE, and LiFSI-ULE electrolytes, respectively (Figure S8).

To gain deeper insight into the disparate electrochemical behaviors, the coin cells were disassembled after 100 cycles for post-mortem analysis of the cycled Li metal anodes. Scanning electron microscopy (SEM) images revealed a distinct morphological contrast on the Li surfaces, consisting of dense, chunk-like regions with low contrast and porous, moss-like areas with high contrast (Figure 2c–e). Energy-dispersive X-ray spectroscopy (EDS) confirmed the presence of C, N, O, F, and S in both regions, originating from the decomposition of electrolyte components and polysulfides (Figures 2f, S9 and S10). Notably, the porous moss-like areas exhibited a significantly higher sulfur-to-fluorine (S/F) ratio (4.3) compared to the compact regions (2.4), indicating severe localized corrosion caused by polysulfides. The corrosion ratio was subsequently quantified by measuring the relative area of these distinct morphologies (Figure 2g–i). A strong correlation was established between the electrochemically derived CE and the physically observed corrosion: a higher corrosion ratio directly corresponded to a CE less than 100%. This confirms that the anomalous CE values are primarily a consequence of polysulfide shuttle effects and the resulting corrosion of the Li metal anode.

To gain molecular-level insight into the corrosion mechanism and the protective role of LiFSI, S 2p and F 1 s X-ray photoelectron spectroscopy (XPS) analyzes were conducted on cycled Li metal anodes. In the S 2p spectra (Figure 3a), signals at binding energies above 165 eV correspond to high-valence species such as S-F and S-O, while those below 165 eV are attributed to low-valence reduction products like Li_2S_2 and Li_2S [26], which form from the parasitic reaction of polysulfides with the Li metal. Notably, the anode cycled in the LiFSI-ULE exhibited a significantly lower intensity of these Li_2S_2/Li_2S peaks compared

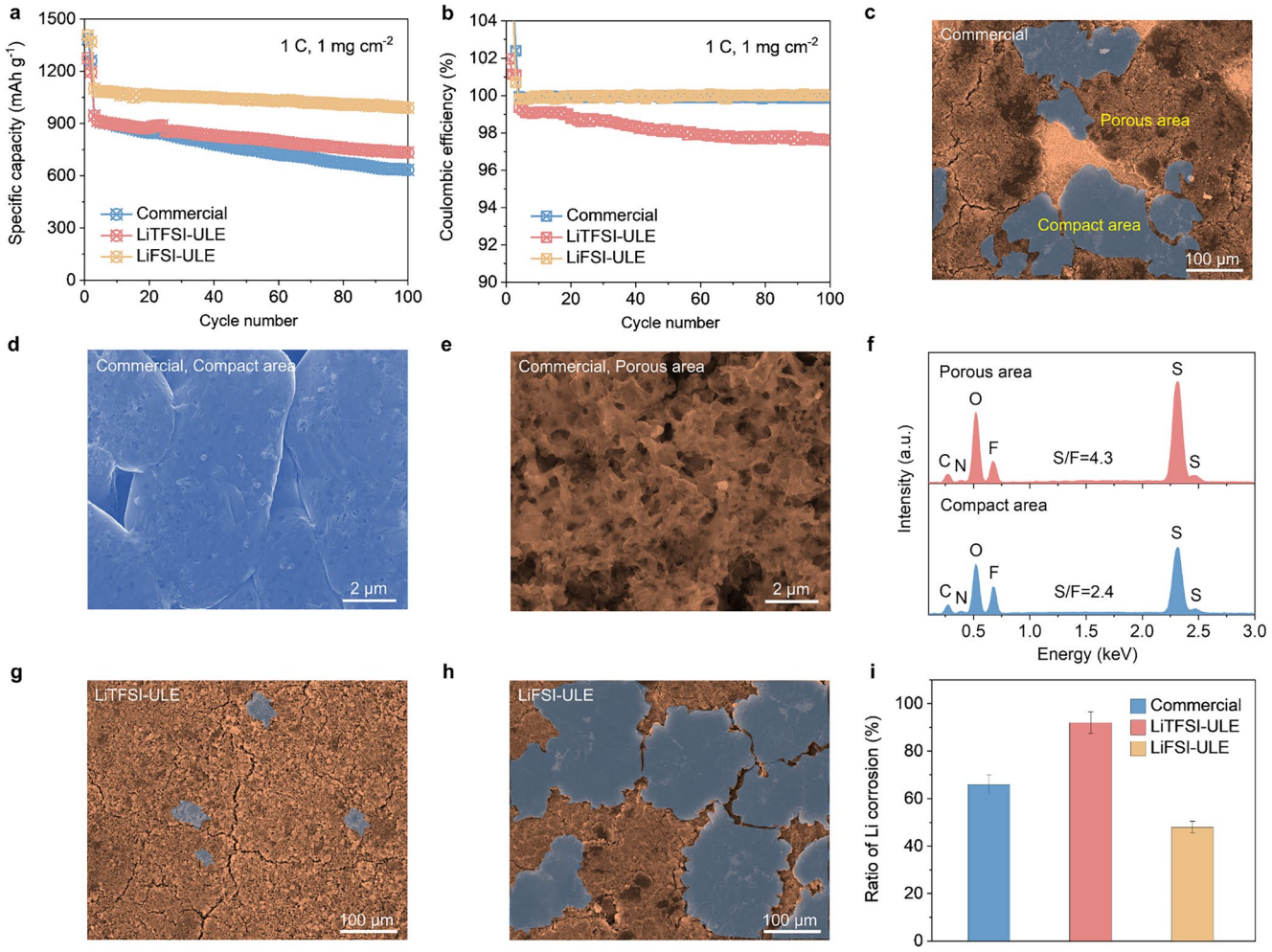

FIGURE 2 | Corrosion behavior of Li metal anodes in Li-S batteries with different electrolytes. (a) Cycling stability and (b) corresponding CE at 1 C (1 C = 1000 mA g^{-1}). (c–e) Representative SEM images at different magnifications and (f) the corresponding EDS spectrum of the cycled Li metal anode from the cell with commercial electrolyte, revealing severe corrosion and the composition of the corrosion layer. SEM images of cycled Li metal anodes from cells with (g) LiTFSI-ULE and (h) LiFSI-ULE electrolytes. (i) Quantitative analysis of the Li metal corrosion areal ratio derived from SEM image analysis, confirming the significant mitigation of corrosion enabled by the LiFSI-ULE electrolytes.

to anodes cycled in commercial and LiTFSI-ULE electrolytes, providing direct evidence of suppressed Li metal corrosion. The F 1s spectra (Figure 3b) further elucidate the composition of the SEI. The SEI formed in the commercial and LiTFSI-ULE electrolytes contained a mixture of organic C-F (688.5 eV) and inorganic LiF (685.2 eV) compounds. In sharp contrast, the SEI derived from the LiFSI-ULE was composed predominantly of inorganic LiF, which also exhibited the highest relative content among all samples (Figure 3c).

Electrochemical impedance spectroscopy (EIS) measurements and self-discharge tests provided further evidence of the superior stability afforded by the LiFSI-ULE. The bulk electrolyte resistance (R_E) in the LiTFSI-ULE (13 Ω) was substantially higher than in both the commercial electrolyte (3 Ω) and the LiFSI-ULE (2 Ω) (Figures 3d and S11). This elevated R_E is attributed to the increased viscosity and decreased conductivity caused by the substantial accumulation of polysulfides in the LiTFSI-ULE. Concurrently, the resistance from the solid electrolyte interphase (R_{SEI}) was lowest in the LiFSI-ULE, providing direct evidence of less severe corrosion. These findings were corroborated by 120-h self-discharge tests, in which the S cathode in the LiFSI-ULE maintained the highest open-circuit potential and exhibited the lowest resistance (Figure S12). Overall, the inorganic LiF-rich SEI formed in the LiFSI-ULE is mechanically robust and electrically insulating. It functions as an effective protective layer that suppresses parasitic reactions between polysulfides and the Li metal anode, leading to markedly reduced corrosion and mitigated shuttle effects, as illustrated in the mechanistic diagrams (Figure 3e,f).

2.3 | Kinetics of Polysulfide Conversion and Li_2S Deposition

The sluggish conversion kinetics of long-chain lithium polysulfides to Li_2S represent a critical rate-determining step in Li-S batteries, directly governing the ultimate capacity utilization of the S cathode. To investigate this process in depth, we assembled Li-Li_2S_6 cells using carbon felts as conductive substrates and a Li_2S_6-containing catholyte as the active material. All cells exhibited a single, distinct discharge plateau at approximately

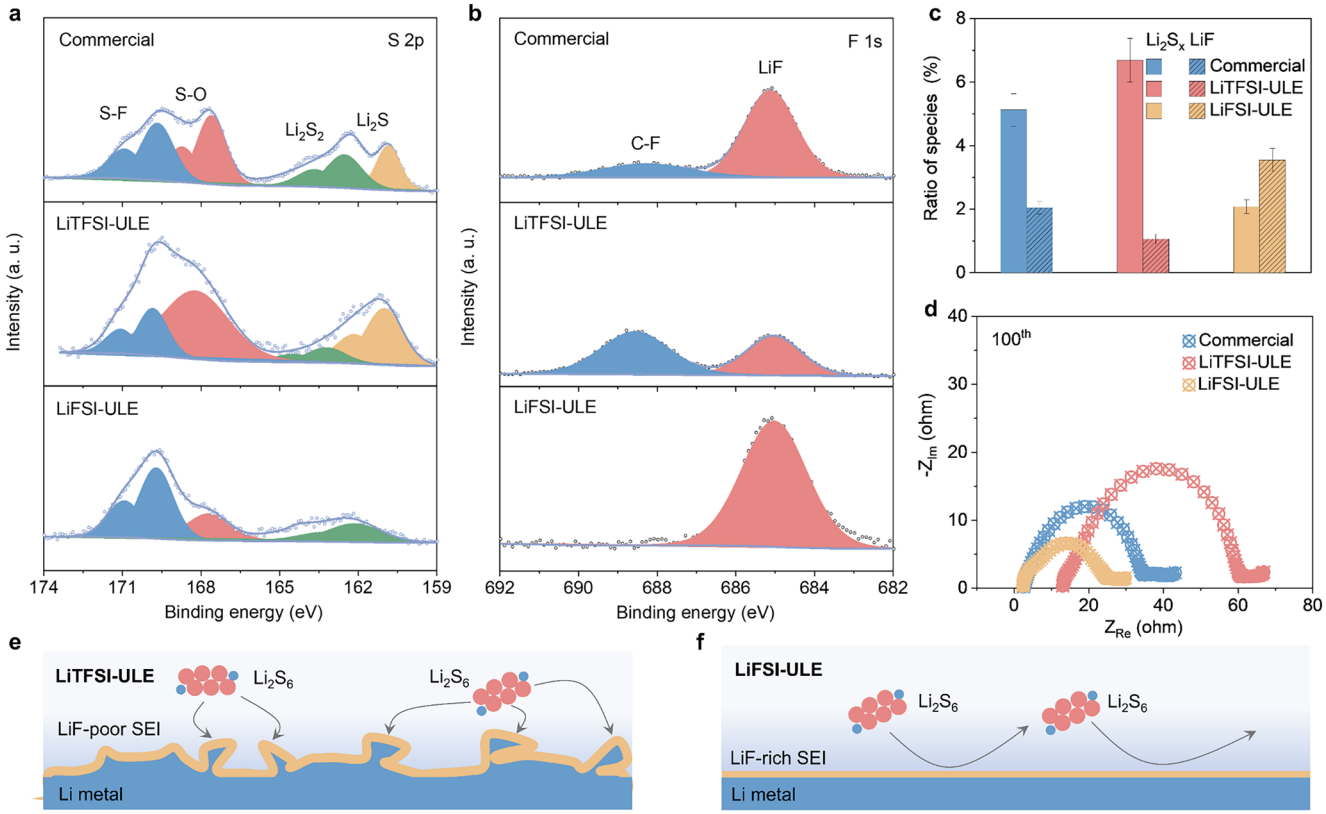

FIGURE 3 | Mechanism of Li metal anode corrosion and interfacial evolution in Li-S batteries with different electrolytes. High-resolution XPS spectra of cycled Li anodes in the (a) S 2p and (b) F 1 s regions for the commercial, LiTFSI-ULE, and LiFSI-ULE electrolytes. (c) Atomic ratio of Li_2S_x (Li_2S/Li_2S_2) to LiF derived from XPS quantification, reflecting the composition of the SEI. (d) Nyquist plots after 100 cycles. Schematic diagrams illustrating the corrosion process of the Li anode and the role of the SEI in (e) LiTFSI-ULE and (f) LiFSI-ULE electrolytes, emphasizing the function of LiF-rich or LiF-deficient interfaces in polysulfide trapping and corrosion suppression.

2.1 V during the initial cycle, corresponding to the conversion of Li_2S_6 to Li_2S (Figure 4a). Remarkably, the cell employing the LiFSI-ULE delivered a significantly higher specific capacity of 1169 mAh g^{-1} with a reduced overpotential (plateau at 2.11 V), markedly outperforming the cell with LiTFSI-ULE, which achieved only 858 mAh g^{-1} with a larger overpotential (plateau at 2.08 V). This enhanced performance is attributed to the higher donor number of the FSI^- anion (10.7 kcal mol^{-1}) compared to the $TFSI^-$ anion (5.4 kcal mol^{-1}) [27–30]. The elevated donor number of FSI^- facilitates superior solvation and improved solubility of polysulfides within the electrolyte (Figure S13). These dissolved polysulfide species subsequently act as effective redox mediators, dramatically accelerating the conversion kinetics and thereby enhancing the overall capacity utilization of the S cathode [31].

The passivation kinetics of the current collector, a critical factor governing S cathode capacity utilization, were quantitatively assessed using chronoamperometry (CA) tests conducted at a constant potential of 2 V (Figure 4b). In all CA profiles, the current response exhibits a characteristic dynamic: an initial decrease due to the reduction of Li_2S_6, followed by a subsequent increase attributed to the progressive nucleation and growth of Li_2S [32]. The current reaches a distinct maximum value (I_m), after which it declines as the conductive carbon surface becomes progressively passivated by the electrically insulating Li_2S deposit. The time taken to reach this current maximum (t_m) serves as a direct metric for the passivation speed—a shorter t_m indicates faster surface coverage and thus poorer kinetics. To provide a more fundamental kinetic parameter, the lateral growth rate of Li_2S was further quantified by applying the Bewick-Fleischmann-Thirsk model to the CA data [28]. The calculated lateral growth rate in the LiFSI-ULE ($5.22\times10^{-10}\,s^{-2}$) was substantially smaller than that in the LiTFSI-ULE ($10.75\times10^{-10}\,s^{-2}$) (Figure 4c). This marked reduction confirms that the high donor number of the FSI^- anion effectively moderates the passivation kinetics at the electrode-electrolyte interface, thereby facilitating a more controlled and favorable deposition process.

The differing passivation kinetics, quantified by chronoamperometry, are directly reflected in the distinct morphological evolution of the deposited Li_2S. After discharge to 1.7 V, SEM analysis reveals a striking contrast: a two-dimensional (2D), film-like Li_2S layer forms on the carbon fiber current collector in the LiTFSI-ULE, whereas three-dimensional (3D), particulate Li_2S deposits are observed in the LiFSI-ULE (Figure 4d,e). This morphological difference is further supported by EDS mapping, which confirms the uniform composition and distribution of the S deposits (Figure S14). The 2D film morphology in the LiTFSI-ULE is characteristic of rapid lateral growth, leading to quick passivation of the conductive substrate and, consequently, inferior capacity utilization. In contrast, the slower lateral growth kinetics enabled by the high donor number of LiFSI promote 3D, island-like deposition. This morphology is highly advantageous,

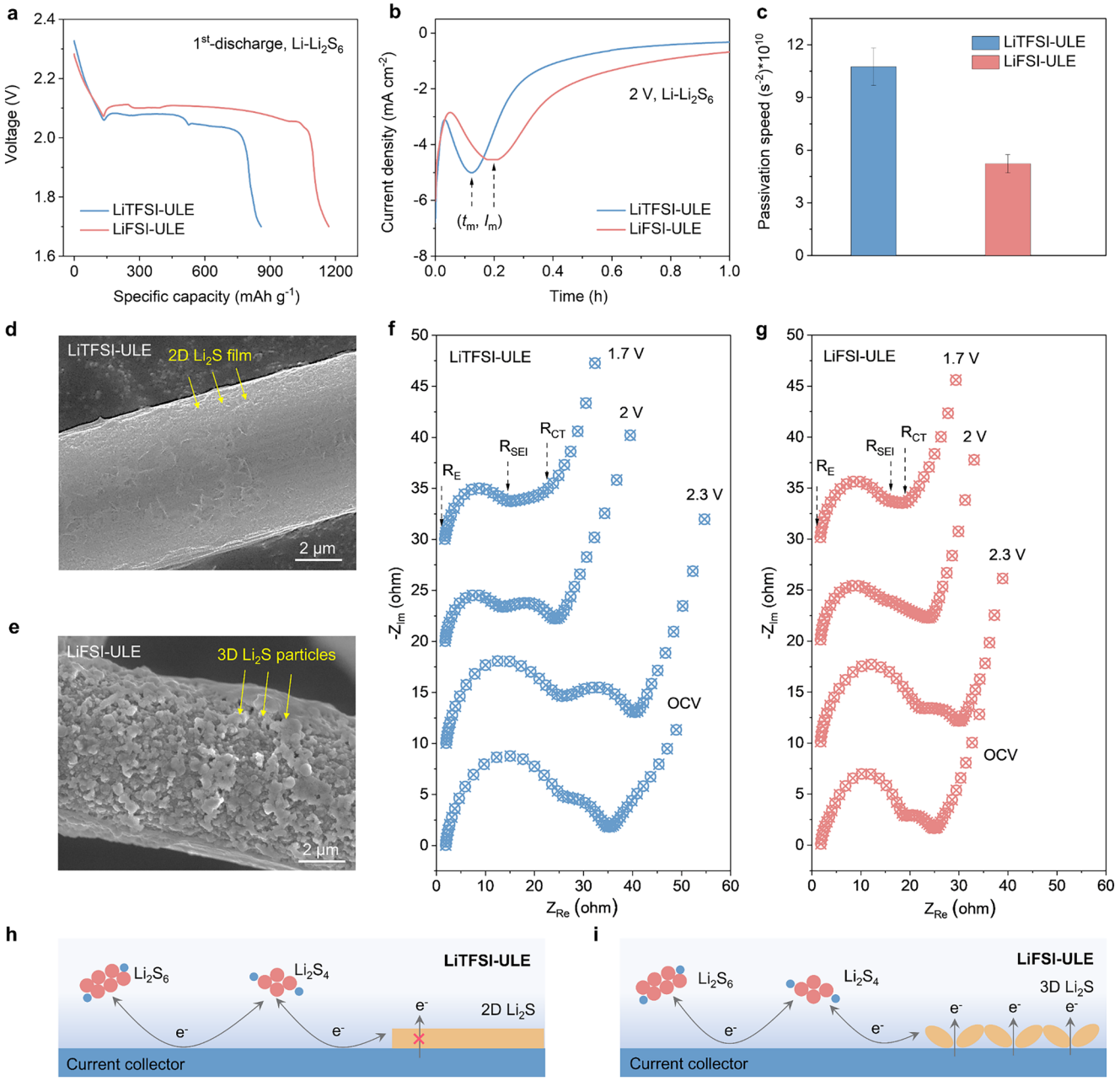

FIGURE 4 | Conversion kinetics and nucleation behavior of Li_2S in LiTFSI-ULE and LiFSI-ULE electrolytes. (a) Discharge profiles of Li-Li_2S_6 cells. (b) Current transients during potentiostatic discharge at 2.0 V and (c) the corresponding lateral growth velocity of Li_2S, indicating the nucleation and growth rate. (d, e) Corresponding morphological characterization of the deposited Li_2S, revealing a 2D film-like structure in LiTFSI-ULE and a 3D particulate morphology in LiFSI-ULE. (f, g) Nyquist plots measured at different potentials (OCV, 2.3 V, 2.0 V, 1.7 V). (h, i) Schematic models illustrating the proposed Li_2S deposition mechanisms: A conformal 2D film leading to passivation in LiTFSI-ULE, versus a porous 3D growth facilitating continuous conversion in LiFSI-ULE.

as it maintains a greater electrochemically active surface area on the current collector for a longer duration during discharge, facilitating continued electrochemical reactions and significantly enhancing the ultimate S utilization and capacity output of the cathode.

To comprehensively evaluate the dynamic evolution of interfacial impedance and further corroborate the enhanced kinetics, EIS was conducted at various characteristic potentials throughout the discharge process (OCV: initial state; 2.3 V: upper plateau; 2 V: lower plateau; 1.7 V: full discharge). The Nyquist plots (Figures 4f,g and S15) reveal a progressive decrease in both the bulk electrolyte resistance (R_E) and the solid electrolyte interphase resistance (R_{SEI}) for all electrolytes after the initial state. This systematic reduction in impedance is attributed to the formation of soluble polysulfide species, which act as redox mediators to catalytically enhance the overall reaction kinetics of the S cathode. Notably, the LiFSI-ULE consistently demonstrated lower resistance values across all measured potentials and temperatures (Figure S16), alongside a larger redox current in Li_2S_6 symmetric cells (Figure S17). Furthermore, analysis via the galvanostatic intermittent titration technique (GITT) and cyclic

voltammetry (CV) confirmed a higher Li^+ diffusion coefficient for the LiFSI-ULE system (Figures S18 and S19). This comprehensive suite of kinetic evidence definitively demonstrates the superior reaction kinetics enabled by the LiFSI-ULE. Overall, the high donor number of the FSI^- anion effectively modulates the deposition process by slowing the lateral growth rate of insulating Li_2S. This unique property facilitates a favorable 3D growth mode, which is crucial for achieving high active material utilization and exceptional capacity output in the S cathode, as conceptually illustrated in Figure 4h,i.

2.4 | Electrochemical Performance Under Practical Conditions

The practical electrochemical performance of the LiFSI-ULE was rigorously evaluated under demanding conditions representative of real-world applications, specifically using high-sulfur-loading cathodes (~5 mg cm^{-2}, ~5.5 mAh cm^{-2}) and a lean E/S ratio of 5 μL mg^{-1}. The S cathode exhibited exceptional cycling stability, delivering a high initial capacity (1180 mAh g^{-1}) and maintaining 70.63% capacity retention after 200 cycles at a rate of 0.5 C, coupled with a near-ideal average CE of 99.14% (Figures 5a and S20). This outstanding performance is demonstrably superior to all previously reported results employing various electrolyte modification strategies, including low-density electrolytes [10, 14, 33, 34], highly solvating electrolytes [35–37], electrolytes designed for Li anode stability [31, 38, 39], and those incorporating redox mediators [40–42] or ingredients [43–48], when compared under analogous stringent criteria (E/S ≤ 5 μL mg^{-1} and S loading ≥ 4 mg cm^{-2}, Figure 5b and Table S1). Furthermore, the cathode demonstrated remarkable rate capability and consistent cycling performance across a range of other S loadings and testing conditions, underscoring the robustness and versatility of the LiFSI-ULE (Figures S21 and S22).

To further validate the practical application potential of the LiFSI-ULE under conditions closely resembling those of commercial batteries, we assembled and evaluated Li-S pouch cells configured with a thin Li metal anode (100 μm), a

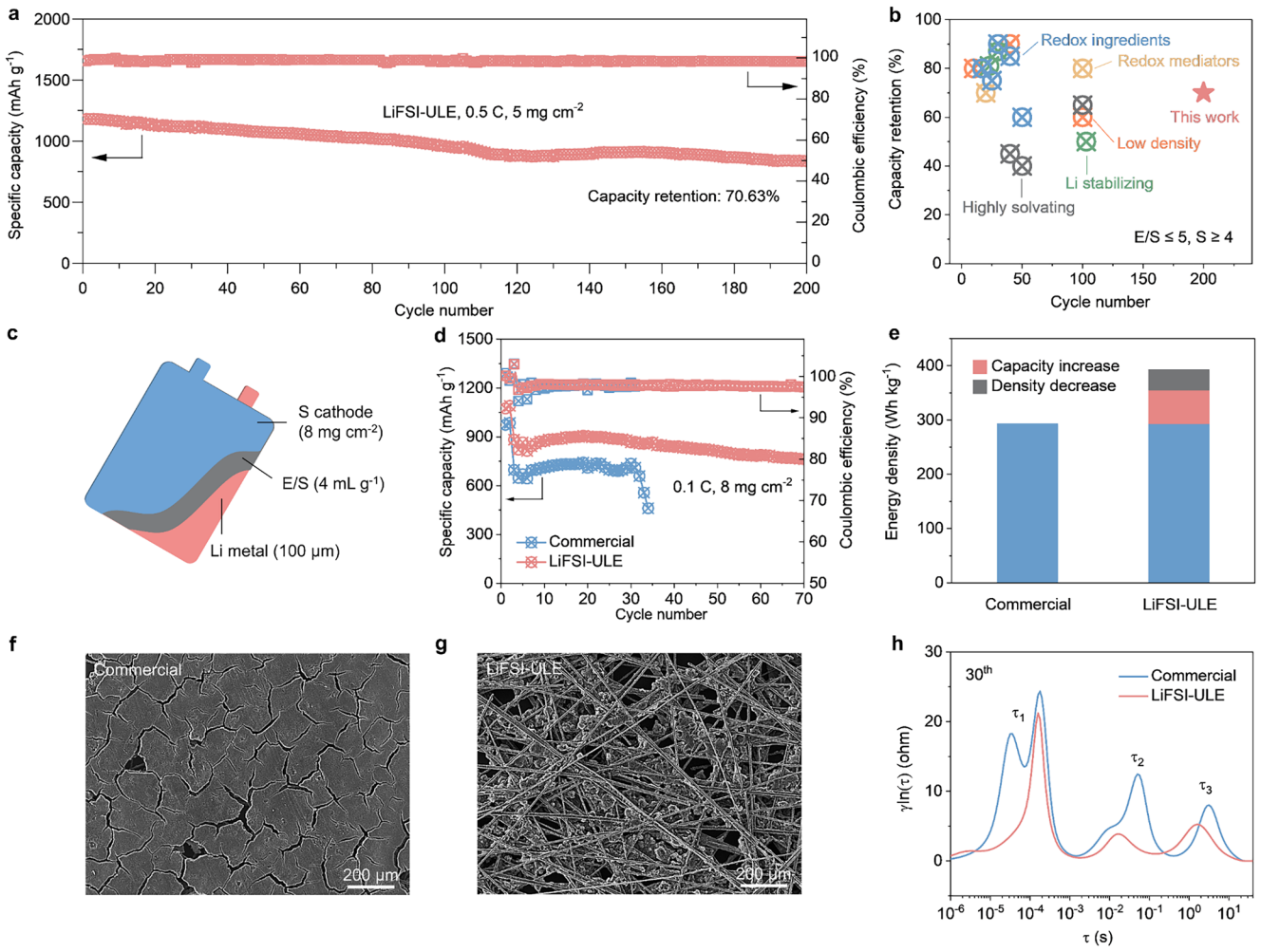

FIGURE 5 | Comprehensive electrochemical evaluation of high-loading Li-S batteries and pouch cells employing the LiFSI-ULE electrolyte. (a) Long-term cycling performance of a high-sulfur-loading cathode (5 mg cm^{-2}) at 0.5 C. (b) Comparison of the cycling stability in (a) with performance data from previously reported literature, highlighting its competitive advantage. (c) Schematic illustration of the pouch cell configuration used in this study. (d, e) Cycling performance and the corresponding practical energy density achieved in the Li-S pouch cell. (f, g) Post-cycling SEM morphologies of S cathodes retrieved from cells using the (f) commercial electrolyte and (g) LiFSI-ULE. (h) Distribution of relaxation times (DRT) deconvoluting the interfacial processes.

high-sulfur-loading cathode (~8 mg cm^{-2}), and a lean E/S ratio of 4 μL mg^{-1} (Figure 5c). The pouch cell employing a conventional commercial electrolyte exhibited a severely limited cycle life, functioning for only approximately 30 cycles with a low capacity utilization of 993 mAh g^{-1} (Figures 5d and S23). In stark contrast, the pouch cell utilizing the LiFSI-ULE demonstrated dramatically improved performance, delivering a much higher specific capacity of 1095 mAh g^{-1} and sustaining stable operation for over 70 cycles. This superior performance directly translates to a substantial gain in practical energy density, reaching 394 Wh kg^{-1} for the LiFSI-ULE cell compared to just 293 Wh kg^{-1} for the cell with commercial electrolyte, as quantified in Figure 5e, Tables S2 and S3. This 34.5% enhancement in energy density is attributed to the synergistic combination of higher capacity utilization and the significantly reduced mass contribution of the ultralight electrolyte itself.

Post-cycling analysis revealed the root cause of failure in the commercial electrolyte: severe aggregation of the S cathode material, which electrically isolated active material from the current collector and led to increased polarization and rapid capacity fade (Figures 5f and S24). Conversely, the S cathode cycled in the LiFSI-ULE largely retained a mono-dispersed morphology, ensuring maintained electrical connectivity and efficient reaction kinetics (Figure 5g). Further kinetic analysis via the distribution of relaxation times confirmed the superiority of the LiFSI-ULE, showing that all characteristic time constants (τ_1, τ_2, τ_3) exhibited both smaller values and lower associated impedances, indicating faster and more efficient reaction processes throughout the discharge cycle (Figures 5h and S25).

3 | Conclusions

In summary, we have successfully designed and demonstrated a ULE based on LiFSI that effectively addresses the critical challenges facing high-energy-density Li-S batteries. The formulated LiFSI-ULE simultaneously achieves an ultralow density of 0.89 g mL^{-1} and a high Li^+ conductivity of 7.05 mS cm^{-1}. The strategic selection of the LiFSI salt confers dual synergistic mechanisms: on the Li metal anode, it facilitates the formation of a robust, LiF-rich SEI that effectively suppresses polysulfide corrosion and shuttle effects, thereby significantly enhancing CE and cycle life. Concurrently, on the S cathode side, the high donor number of the FSI^- anion improves polysulfide solubility, accelerating conversion kinetics and promoting a favorable 3D deposition of Li_2S, which leads to markedly improved S utilization. Consequently, under practical conditions—a high S loading (5 mg cm^{-2}) and a lean E/S ratio (4 μL mg^{-1})—the LiFSI-ULE enables a high initial capacity of 1180 mAh g^{-1} and outstanding capacity retention of 70.63% after 200 cycles at 0.5 C. This performance surpasses all previously reported results employing electrolyte modification strategies under comparable stringent test conditions. Crucially, in practical pouch cell configurations, the use of LiFSI-ULE results in a 34.5% higher energy density (394 Wh kg^{-1}) and a 133% longer cycle life compared to conventional electrolytes. This work not only successfully extends the application of LiFSI from high-voltage Li metal batteries to the Li-S system but also provides a viable and promising pathway toward the realization of long-cycling, high-energy-density energy storage solutions.

Author Contributions

Junhua Zhou: writing, visualization, data analysis. **Yufeng Luo:** characterization. **Chao Wang:** characterization. **Chuan Xie:** data analysis. **Huimin Wang:** data analysis. **Yanpeng Guo:** editing. **Yongqiang Yang:** editing. **Zhibo Li:** data analysis. **Shujing Wen:** data analysis. **Jiehua Cai:** data analysis. **Qiyao Huang:** editing, supervision. **Zijian Zheng:** writing, editing, supervision, resources, conceptualization.

Acknowledgments

The authors acknowledge the financial support from Guangdong Hong Kong Technology Cooperation Funding Scheme (GHP/047/20GD), National Natural Science Foundation of China/Hong Kong Research Grants Council (CRS_PolyU504/22), Research Grants Council (R5019-22), National Natural Science Foundation of China (52203318, 52401268), and the Hong Kong Polytechnic University (1-W22M, 1-BDYU).

Funding

This work was supported by National Natural Science Foundation of China (Grants 52203318 and 52401268), Guangdong Hong Kong Technology Cooperation Funding Scheme (Grant GHP/047/20GD), Hong Kong Polytechnic University (Grants 1-BDYU and 1-W22M), Research Grants Council (Grant R5019-22) and National Natural Science Foundation of China/Hong Kong Research Grants Council (Grant CRS_PolyU504/22).

Conflicts of Interest

Zijian Zheng is Editor-in-Chief of EcoMat and co-author of this article. He was excluded from the peer-review process and all editorial decisions related to the acceptance and publication of this article. Peer review was handled independently by Associate Editor Qiang Zhang to minimize bias. The other authors declare no conflicts of interest.

Data Availability Statement

The data that support the findings of this study are available from the corresponding author upon reasonable request.

References

1. P. G. Bruce, S. A. Freunberger, L. J. Hardwick, and J.-M. Tarascon, "Li–O_2 and Li–S Batteries With High Energy Storage," *Nature Materials* 11 (2011): 19–29.

2. J. W. Choi and D. Aurbach, "Promise and Reality of Post-Lithium-Ion Batteries With High Energy Densities," *Nature Reviews Materials* 1 (2016): 16013.

3. X. Ji, K. T. Lee, and L. F. Nazar, "A Highly Ordered Nanostructured Carbon–Sulphur Cathode for Lithium–Sulphur Batteries," *Nature Materials* 8 (2009): 500.

4. H. Zhao, Y. Wang, Y. Jiang, et al., "Designing Thin and Lightweight 3D Metallized Current Collectors With Functional Interfaces for High-Energy-Density Lithium-Sulfur Batteries," *EcoMat* 7 (2025): e70022.

5. Q. Pang, X. Liang, C. Y. Kwok, and L. F. Nazar, "Advances in Lithium–Sulfur Batteries Based on Multifunctional Cathodes and Electrolytes," *Nature Energy* 1 (2016): 16132.

6. A. Manthiram, Y. Fu, S.-H. Chung, C. Zu, and Y.-S. Su, "Rechargeable Lithium–Sulfur Batteries," *Chemical Reviews* 114 (2014): 11751.

7. Q. Pang, A. Shyamsunder, B. Narayanan, C. Y. Kwok, L. A. Curtiss, and L. F. Nazar, "Tuning the Electrolyte Network Structure to Invoke Quasi-Solid State Sulfur Conversion and Suppress Lithium Dendrite Formation in Li–S Batteries," *Nature Energy* 3 (2018): 783–791.

8. H. Raza, J. Cheng, C. Lin, S. Majumder, G. Zheng, and G. Chen, "High-Entropy Stabilized Oxides Derived via a Low-Temperature Template Route for High-Performance Lithium-Sulfur Batteries," *EcoMat* 5 (2023): e12324.

9. S. Dörfler, H. Althues, P. Härtel, T. Abendroth, B. Schumm, and S. Kaskel, "Challenges and Key Parameters of Lithium-Sulfur Batteries on Pouch Cell Level," *Joule* 4 (2020): 539–554.

10. T. Liu, H. Li, J. Yue, et al., "Ultralight Electrolyte for High-Energy Lithium–Sulfur Pouch Cells," *Angewandte Chemie, International Edition* 60 (2021): 17547.

11. J. Zhou, C. Zhang, C. Xie, et al., "A Low-Cost $Al(OH)_3$-Modified Fire-Retardant and Shuttle-Limiting Separator for Safe and Stable Lithium–Sulfur Batteries," *Advanced Energy Materials* 14 (2023): 2303063.

12. J. Chen, Y. Fu, and J. Guo, "Development of Electrolytes Under Lean Condition in Lithium-Sulfur Batteries," *Advanced Materials* 36 (2024): 2401263.

13. Y. Liu, Y. Elias, J. Meng, et al., "Electrolyte Solutions Design for Lithium-Sulfur Batteries," *Joule* 5 (2021): 2323–2364.

14. T. Liu, Z. Shi, H. Li, et al., "Low-Density Fluorinated Silane Solvent Enhancing Deep Cycle Lithium–Sulfur Batteries' Lifetime," *Advanced Materials* 33 (2021): 2102034.

15. J. Feng, T. Liu, H. Li, Y.-S. Hu, H. Mao, and L. Suo, "Ultralight Electrolyte With Protective Encapsulation Solvation Structure Enables Hybrid Sulfur-Based Primary Batteries Exceeding 660 Wh/kg," *Journal of the American Chemical Society* 146 (2024): 3755–3763.

16. Z. Han, S. Li, M. Sun, et al., "Fluorobenzene Diluted Low-Density Electrolyte for High-Energy Density and High-Performance Lithium-Sulfur Batteries," *Journal of Energy Chemistry* 68 (2022): 752.

17. T. Jin, X.-Y. Li, M. Zhao, et al., "Promoting the Rate Performances of Weakly Solvating Electrolyte-Based Lithium–Sulfur Batteries," *Angewandte Chemie* 64 (2025): e202504898.

18. Z.-X. Chen, J.-J. Zhao, G.-Y. Fang, et al., "Accelerating the Sulfur Redox Kinetics in Weakly-Solvating Lithium–Sulfur Batteries Under Lean-Electrolyte Conditions," *Energy Storage Materials* 83 (2025): 104502.

19. Y. Han, X. Duan, Y. Li, L. Huang, D. Zhu, and Y. Chen, "Effects of Sulfur Loading on the Corrosion Behaviors of Metal Lithium Anode in Lithium–Sulfur Batteries," *Materials Research Bulletin* 68 (2015): 160.

20. X.-Y. Li, S. Feng, Y.-W. Song, et al., "Kinetic Evaluation on Lithium Polysulfide in Weakly Solvating Electrolyte Toward Practical Lithium–Sulfur Batteries," *Journal of the American Chemical Society* 146 (2024): 14754.

21. D. Lu, R. Li, M. M. Rahman, et al., "Ligand-Channel-Enabled Ultrafast Li-Ion Conduction," *Nature* 627 (2024): 101.

22. X.-Y. Li, B.-Q. Li, S. Feng, et al., "Two-Stage Solvation of Lithium Polysulfides in Working Lithium–Sulfur Batteries," *Journal of the American Chemical Society* 147 (2025): 15435.

23. G. M. Hobold, J. Lopez, R. Guo, et al., "Moving Beyond 99.9% Coulombic Efficiency for Lithium Anodes in Liquid Electrolytes," *Nature Energy* 6 (2021): 951–960.

24. Y.-W. Song, L. Shen, X.-Y. Li, et al., "Phase Equilibrium Thermodynamics of Lithium–Sulfur Batteries," *Nature Chemical Engineering* 1 (2024): 588–596.

25. Q. Zhao, X. Liu, J. Zheng, et al., "Designing Electrolytes With Polymerlike Glass-Forming Properties and Fast Ion Transport at Low Temperatures," *Proceedings of the National Academy of Sciences of the United States of America* 117 (2020): 26053–26060.

26. W. Hua, T. Shang, H. Li, et al., "Optimizing the P Charge of S in P-Block Metal Sulfides for Sulfur Reduction Electrocatalysis," *Nature Catalysis* 6 (2023): 174.

27. X. Wang, Z. Shang, A. Yang, et al., "Combining Quinone Cathode and Ionic Liquid Electrolyte for Organic Sodium-Ion Batteries," *Chem* 5 (2019): 364–375.

28. H. Chu, H. Noh, Y.-J. Kim, et al., "Achieving Three-Dimensional Lithium Sulfide Growth in Lithium-Sulfur Batteries Using High-Donor-Number Anions," *Nature Communications* 10 (2019): 188.

29. M. Baek, H. Shin, K. Char, and J. W. Choi, "New High Donor Electrolyte for Lithium–Sulfur Batteries," *Advanced Materials* 32 (2020): 2005022.

30. L. Johnson, C. Li, Z. Liu, et al., "The Role of LiO_2 Solubility in O_2 Reduction in Aprotic Solvents and Its Consequences for Li–O_2 Batteries," *Nature Chemistry* 6 (2014): 1091.

31. L.-P. Hou, X.-Q. Zhang, N. Yao, et al., "An Encapsulating Lithium-Polysulfide Electrolyte for Practical Lithium–Sulfur Batteries," *Chem* 8 (2022): 1083–1098.

32. R. Liu, Z. Wei, L. Peng, et al., "Establishing Reaction Networks in the 16-Electron Sulfur Reduction Reaction," *Nature* 626 (2024): 98–104.

33. Y. Zhao, J. Zhang, and J. Guo, "Cathode–Electrolyte Interfacial Processes in Lithium||Sulfur Batteries Under Lean Electrolyte Conditions," *ACS Applied Materials & Interfaces* 13 (2021): 31749–31755.

34. H. Cheng, S. Zhang, B. Zhang, and Y. Lu, "*n*-Hexane Diluted Electrolyte With Ultralow Density Enables Li–S Pouch Battery Toward >400 Wh kg^{-1}," *Small* 19 (2022): 2206375.

35. A. Gupta, A. Bhargav, and A. Manthiram, "Evoking High-Donor-Number-Assisted and Organosulfur-Mediated Conversion in Lithium–Sulfur Batteries," *ACS Energy Letters* 6 (2020): 224.

36. H. Pan, K. S. Han, M. H. Engelhard, et al., "Addressing Passivation in Lithium–Sulfur Battery Under Lean Electrolyte Condition," *Advanced Functional Materials* 28 (2018): 1707234.

37. Y. Chen, H. Zhang, W. Xu, et al., "Polysulfide Stabilization: A Pivotal Strategy to Achieve High Energy Density Li–S Batteries With Long Cycle Life," *Advanced Functional Materials* 28 (2017): 1704987.

38. X.-Q. Zhang, Q. Jin, Y.-L. Nan, et al., "Electrolyte Structure of Lithium Polysulfides With Anti-Reductive Solvent Shells for Practical Lithium-Sulfur Batteries," *Angewandte Chemie (International Ed. in English)* 60 (2021): 15503.

39. L. Zheng, L.-P. Hou, N. Yao, et al., "Correlating Polysulfide Solvation Structure With Electrode Kinetics Towards Long-Cycling Lithium-Sulfur Batteries," *Angewandte Chemie (International Ed. in English)* 62 (2023): e202309968.

40. M. Zhao, H.-J. Peng, J.-Y. Wei, et al., "Dictating High-Capacity Lithium–Sulfur Batteries Through Redox-Mediated Lithium Sulfide Growth (Small Methods 6/2020)," *Small Methods* 4 (2019): 1900344.

41. H. Ye, J. Sun, X. F. Lim, Y. Zhao, and J. Y. Lee, "Mediator–Assisted Catalysis of Polysulfide Conversion for High–Loading Lithium–Sulfur Batteries Operating Under the Lean Electrolyte Condition," *Energy Storage Materials* 38 (2021): 338–343.

42. Z. Shen, Q. Gao, X. Zhu, et al., "In-Situ Free Radical Supplement Strategy for Improving the Redox Kinetics of Li-S Batteries," *Energy Storage Materials* 57 (2023): 299.

43. S. Chen, Y. Gao, Z. Yu, M. L. Gordin, J. Song, and D. Wang, "High Capacity of Lithium-Sulfur Batteries at Low Electrolyte/Sulfur Ratio Enabled by an Organosulfide Containing Electrolyte," *Nano Energy* 31 (2017): 418.

44. M. Zhao, B.-Q. Li, X. Chen, J. Xie, H. Yuan, and J.-Q. Huang, "Redox Comediation With Organopolysulfides in Working Lithium-Sulfur Batteries," *Chem* 6 (2020): 3297–3311.

45. W. Zhang, F. Ma, Q. Wu, et al., "Dual-Functional Organotelluride Additive for Highly Efficient Sulfur Redox Kinetics and Lithium Regulation in Lithium–Sulfur Batteries," *Energy & Environmental Materials* 6 (2022): e12369.

46. M. Zhao, X.-Y. Li, X. Chen, et al., "Promoting the Sulfur Redox Kinetics by Mixed Organodiselenides in High-Energy-Density Lithium–Sulfur Batteries," *EScience* 1 (2021): 44.

47. M. Zhao, X. Chen, X.-Y. Li, B.-Q. Li, and J.-Q. Huang, "An Organodiselenide Comediator to Facilitate Sulfur Redox Kinetics in Lithium–Sulfur Batteries," *Advanced Materials* 33 (2021): 2007298.

48. W. Guo, W. Zhang, Y. Si, D. Wang, Y. Fu, and A. Manthiram, "Artificial Dual Solid-Electrolyte Interfaces Based on In Situ Organothiol Transformation in Lithium Sulfur Battery," *Nature Communications* 12 (2021): 3031.

Supporting Information

Additional supporting information can be found online in the Supporting Information section. **Data S1:** eom270050-sup-0001-Supinfo.docx.